

Maxwell–Hydrodynamic Model for Simulating Nonlinear Terahertz Generation From Plasmonic Metasurfaces

Ming Fang, Zhixiang Huang, *Member, IEEE*, Wei E. I. Sha, *Senior Member, IEEE*, and Xianliang Wu, *Member, IEEE*

Abstract—The interaction between electromagnetic field and plasmonic nanostructures leads to both strong linear and nonlinear behaviors. In this paper, a time-domain hydrodynamic model for describing the motion of electrons in plasmonic nanostructures is presented, in which both surface and bulk nonlinearity are considered. A coupled Maxwell–hydrodynamic system capturing full-wave physics and free-electron dynamics is numerically solved with the parallel finite-difference time-domain method. The validation of the proposed method is presented by simulating a plasmonic metasurface. The linear response is compared with the Drude dispersion model and the nonlinear terahertz emission from a difference-frequency generation process is theoretically analyzed. The work is fundamentally important to design nonlinear plasmonic nanodevices, especially for efficient and broadband THz emitters.

Index Terms—Finite-difference time domain (FDTD), hydrodynamic model, metasurface, nonlinear plasmonic nanodevice, terahertz (THz) emission.

I. INTRODUCTION

PLASMONIC nanostructures play an important role in controlling light, for developing photoluminescence enhancement, optical sensing, solar cell, metamaterials, and optical antenna [1]–[5]. These potential applications arise from surface plasmon resonance (SPR) [6], which is induced by the interaction between plasmonic metal nanostructures and external electromagnetic fields. The SPR can be tailored by modifying the geometry and material of nanostructures [7]. Particularly, they are attractive for their inherent nonlinear optical effects. A variety of photonic functionalities based on the nonlinear effects are reported in recent work, such as optical sensing, ultrashort pulse generation, nanoantenna, and optical signal processing [8]–[11]. However, nonlinear interactions in comparison

with linear interactions are intrinsically weak. They are heavily dependent on the field amplitude of excitation. Consequently, high-power excitation is needed to enlarge nonlinear effects. In experiments, an optical laser is adopted for high-power excitation and strong field enhancement can be achieved by carefully designing plasmonic nanostructures. Due to a low conversion efficiency of high-order nonlinearities, the most exciting and useful effects are the second- and third-order nonlinearities, such as the second-harmonic generation, Kerr effect, third-harmonic generation, and four-wave mixing.

Modeling optical responses of plasmonic nanostructures is a critical step to understand their working principles and perform corresponding designs. For numerical studies, the Drude model is commonly used for describing electron motion in plasmonic materials. However, it is a local-response approximation model that does not account for the nonlinear and nonlocal electromagnetic responses. To solve this problem, a classical electrodynamic framework with suitable approximations and improvements can be used. The nonlinear response can be described with material nonlinear polarization, i.e., $\mathbf{P} = \varepsilon_0 \chi^{(n)} \mathbf{E}^n$, where $\chi^{(n)}$ is the nonlinear susceptibility [12], [13]. Alternatively, a hydrodynamic model in time domain can be used to model nonlinear effects resulting from motion of conduction electrons in metals. The complex nonlinear dynamics is presented in this model, including the magnetic-field contributions from the Lorentz force, convective acceleration, and quantum pressure [14]–[16]. This hydrodynamic model fully considers the linear and nonlinear dynamics of the electron gas and does not rely on the experimentally measured bulk and surface nonlinear susceptibility [17]. Inspired by the above observations, a time-domain implementation of the hydrodynamic model with the classical computational electromagnetics method is desirable.

The finite-difference time domain (FDTD) [18] is one of the most commonly used method to study time-domain behaviors of materials. The FDTD method was originally designed for linear nondispersive dielectric materials, and has been widely used for more than five decades. With the auxiliary differential equation (ADE) technique [19], the FDTD method is extended to the simulation of dispersive materials. The ADE-FDTD method is flexible for modeling complex permittivity functions and nonlinear effects, such as Kerr and Raman effects in nonlinear media [20].

Recently, by using difference-frequency generation, a terahertz (THz) emitter based on a nonlinear metasurface was

Manuscript received April 26, 2017; revised July 25, 2017; accepted August 29, 2017. Date of publication September 12, 2017; date of current version November 22, 2017. This work was supported in part by the National Natural Science Fund for Excellent Young Scholars (61722101), in part by the National Natural Science Foundation of China (61471001 and 61601166), and in part by the Universities Natural Science Foundation of Anhui Province (KJ2017ZD51 and KJ2017ZD02). (*Corresponding author: Ming Fang.*)

M. Fang, Z. Huang, and X. Wu are with the Key Laboratory of Intelligent Computing and Signal Processing, Ministry of Education, Anhui University, Hefei 230039, China (e-mail: ahu_mingfang@yahoo.com; zxhuang@ahu.edu.cn; xlwu@ahu.edu.cn).

W. E. I. Sha is with the College of Information Science and Electronic Engineering, Zhejiang University, Hangzhou 310027, China, and also with the Department of Electrical and Electronic Engineering, The University of Hong Kong, Hong Kong (e-mail: weisha@zju.edu.cn).

Digital Object Identifier 10.1109/JMMCT.2017.2751553

reported [22]. Efficient, broadband and tunable THz emission can be generated in a thin layer of metamaterial with tens of nanometers thickness by an infrared laser pumping. The THz emission intensity from the metamaterial is of the same order as the nonlinear crystals; and the ultrathin THz emitter is free from quasi-phase-matching. However, there is no rigorous and universal numerical model to simulate the nonlinear process. In this paper, a self-consistent parallel ADE-FDTD method is employed in conjugation with the hydrodynamic model to simulate the nonlinear THz emission from plasmonic metasurfaces. Compared to the Maxwell–hydrodynamic model in literature [14], [23] and our previous work [12], [13], [24], a new two-step splitting scheme is proposed to solve the multiphysics model. In [14], [16], [24], the hydrodynamic equations contain nonlinear terms; the explicit scheme cannot be used directly to solve electron velocity and density, except that the approximations of their values at the previous step are employed. Consequently, both the linear and nonlinear responses are solved with the approximations. To keep the accuracy of the simulation, a fine spatial or temporal increment should then be used. In difference, the proposed ADE-FDTD method uses the two-step splitting scheme. The linear effect is explicitly solved by the ADE method and the nonlinear response was explicitly updated with the intermediate value of current obtained from the ADE method. As a result, the linear and nonlinear responses are split and the weak nonlinear signals are not be suppressed by the strong linear pulse signals. The numerical aspects of the proposed model including accuracy, stability, and parallel strategy are presented. To demonstrate the performance of the proposed algorithm, the THz signal emitted from a single periodic layer of gold split-ring resonators on glass is investigated. The numerical simulations in a three-dimensional computational domain yield good agreements with the experimental results in [22].

This paper is organized as follows. The numerical scheme and multiphysics model are introduced in Section II. The nonlinear response of plasmonic metasurfaces is modeled with the proposed scheme in Section III. To benchmark the proposed scheme, the linear transmittance of the metasurface is calculated and the result is compared to the classical Drude model. Then, the THz emission from difference-frequency generation is calculated and compared with theoretical analyses. Finally, this paper is concluded in Section IV.

II. NUMERICAL SCHEME

A. Multiphysics Hydrodynamic Model

The interaction of electromagnetic fields \mathbf{E} and \mathbf{H} with non-magnetic materials is described by the Maxwell's equations

$$\frac{1}{\mu_0} \nabla \times \mathbf{B} = \varepsilon_0 \frac{\partial \mathbf{E}}{\partial t} + \mathbf{J} \quad (1)$$

$$\frac{\partial \mathbf{B}}{\partial t} = -\nabla \times \mathbf{E} \quad (2)$$

where ε_0 and μ_0 are the vacuum permittivity and permeability. \mathbf{J} includes both linear and nonlinear polarization currents, when electromagnetic waves interact with free electron gas in plasmonic materials. The natural dynamics of free electron gas

driven by an external electromagnetic wave is described by the hydrodynamic equation

$$\frac{\partial \mathbf{v}_e}{\partial t} + (\mathbf{v}_e \cdot \nabla) \mathbf{v}_e = -\frac{e}{m} (\mathbf{E} + \mathbf{v}_e \times \mathbf{B}) - \gamma \mathbf{v}_e \quad (3)$$

$$\frac{\partial n_e}{\partial t} + \nabla \cdot (n_e \mathbf{v}_e) = 0 \quad (4)$$

where m and e are the electron mass and electron charge. n_e and \mathbf{v}_e are the electron density and velocity. γ is the phenomenological damping frequency constant. To ensure charge neutrality, the initial electron density n_e is set to be equal to positive ion density n_0 without excitation. $(\mathbf{v}_e \cdot \nabla) \mathbf{v}_e$ term is the convective acceleration of electron gas. Equation (4) is the continuity equation. The electromagnetic field and electron dynamics can be coupled via the macroscopic current density and charge density terms

$$\mathbf{J} = -en_e \mathbf{v}_e \quad (5)$$

$$\rho = e(n_e - n_0). \quad (6)$$

On substituting (5) and (6) into (3) and (4), we get

$$\begin{aligned} \frac{\partial \mathbf{J}}{\partial t} &= \varepsilon_0 \omega_p^2 \mathbf{E} - \gamma \mathbf{J} + \frac{e}{m} (\rho \mathbf{E} - \mathbf{J} \times \mathbf{B}) \\ &+ \nabla \cdot \left(\frac{1}{\rho + \varepsilon_0 m \omega_p^2 / e} \mathbf{J} \mathbf{J} \right) \end{aligned} \quad (7)$$

$$\frac{\partial \rho}{\partial t} - \nabla \cdot \mathbf{J} = 0 \quad (8)$$

where $\omega_p = \sqrt{e^2 n_0 / \varepsilon_0 m}$ is the plasma frequency. Finally, (7) and (8) can be reduced to one equation by substituting $\rho = \varepsilon_0 \nabla \cdot \mathbf{E}$ into them

$$\begin{aligned} \frac{\partial \mathbf{J}}{\partial t} &= \varepsilon_0 \omega_p^2 \mathbf{E} - \gamma \mathbf{J} + \frac{e}{m} [\varepsilon_0 (\nabla \cdot \mathbf{E}) \mathbf{E} - \mathbf{J} \times \mathbf{B}] \\ &+ \nabla \cdot \left(\frac{1}{\varepsilon_0 (\nabla \cdot \mathbf{E}) + \varepsilon_0 m \omega_p^2 / e} \mathbf{J} \mathbf{J} \right). \end{aligned} \quad (9)$$

Equations (1), (2), and (9) form the hydrodynamic model for linear and nonlinear interactions between the electromagnetic wave and free electron gas in plasmonic nanostructures.

B. Computational Grid

In order to solve (1), (2), and (9), a computational grid based on the standard staggered Yee cells is proposed, as seen in Fig. 1. The spatial–temporal dependent \mathbf{E} , \mathbf{H} , and \mathbf{J} are nodally uncollocated in space and staggered in time. The electric field \mathbf{E} is defined at time step $l+1/2$ and is located at the cell face center. Both current density \mathbf{J} and magnetic field \mathbf{H} are defined at the time level l and are located at the cell face centers and the edges, respectively. This grid arrangement captures the properties of fields and charges as well as the cross-coupling effects between free electrons and electromagnetic fields.

C. Two-Step Splitting Scheme

We employ an explicit central difference method to discretize (1) and (2). Considering the sampled time level of \mathbf{J} and the

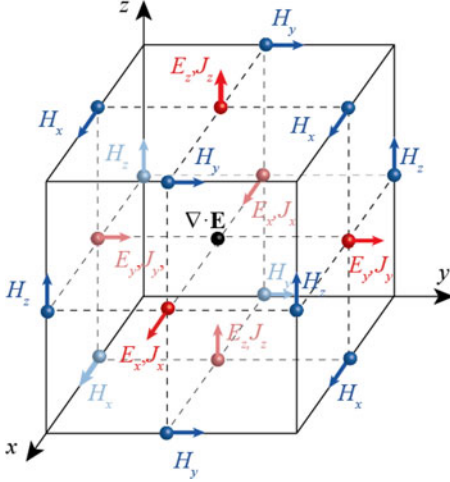


Fig. 1. Yee grids for the Maxwell–hydrodynamic system.

nonlinear properties of (9), a time-splitting scheme is applied for updating \mathbf{J} . We split (9) into two subproblems

$$\frac{\partial \mathbf{J}}{\partial t} = \varepsilon_0 \omega_p^2 \mathbf{E} - \gamma \mathbf{J} \quad (10)$$

$$\frac{\partial \mathbf{J}}{\partial t} = \frac{e}{m} [\varepsilon_0 (\nabla \cdot \mathbf{E}) \mathbf{E} - \mathbf{J} \times \mathbf{B}] + \nabla \cdot \left(\frac{1}{\varepsilon_0 (\nabla \cdot \mathbf{E}) + \varepsilon_0 m \omega_p^2 / e} \mathbf{J} \mathbf{J} \right). \quad (11)$$

Equation (10) is the linear response of electrons as described by the conventional Drude model. Updating \mathbf{J} from the time step l by a central difference scheme, we obtain an intermediate updated current density $\mathbf{J}^{(1)}$ at time step $l+1$

$$\mathbf{J}^{(1),l+1} = \frac{1 - 0.5\Delta t\gamma}{1 + 0.5\Delta t\gamma} \mathbf{J}^l + \frac{\varepsilon_0 \omega_p^2 \Delta t}{1 + 0.5\Delta t\gamma} \mathbf{E}^{l+1/2}. \quad (12)$$

Equation (11) presents the nonlinear response. Since current density \mathbf{J} is defined at the same time level as \mathbf{H} and is at the same location as \mathbf{E} in space. $\varepsilon_0 \nabla \cdot \mathbf{E}$ term in (11) representing the charge density is first calculated at the center of grid. The components are interpolated to approximate the values at the same spatial and temporal point as \mathbf{J} . For example, for updating the x -component of \mathbf{J} , the interpolated $\nabla \cdot \mathbf{E}$ and \mathbf{B} are given by

$$\overline{\nabla \cdot \mathbf{E}}_{i,j+1/2,k+1/2}^{l+1/2} = \frac{1}{2} \left(\nabla \cdot \mathbf{E}_{i+1/2,j+1/2,k+1/2}^{l+1/2} + \nabla \cdot \mathbf{E}_{i-1/2,j+1/2,k+1/2}^{l+1/2} \right) \quad (13)$$

$$\bar{B}_{yi,j+1/2,k+1/2}^{l+1/2} = \frac{1}{4} \left(B_{yi,j+1/2,k}^{l+1} + B_{yi,j+1/2,k+1}^{l+1} + B_{yi,j+1/2,k}^l + B_{yi,j+1/2,k+1}^l \right) \quad (14)$$

$$\bar{B}_{zi,j+1/2,k+1/2}^{l+1/2} = \frac{1}{4} \left(B_{zi,j,k+1/2}^{l+1} + B_{zi,j+1,k+1/2}^{l+1} + B_{zi,j,k+1/2}^l + B_{zi,j+1,k+1/2}^l \right). \quad (15)$$

Meanwhile, \mathbf{J} is interpolated at the time level $l+1/2$ by averaging \mathbf{J}^l and the intermediate current density $\mathbf{J}^{(1),l+1}$

$$\bar{J}_{xi,j+1/2,k+1/2}^{l+1/2} = \frac{1}{2} \left(J_{xi,j+1/2,k+1/2}^l + J_{xi,j+1/2,k+1/2}^{(1),l+1} \right). \quad (16)$$

After explicitly solving (11), the nonlinear intermediate current density $\mathbf{J}^{(2)}$ can be obtained. After getting the second intermediate value of $\mathbf{J}^{(2)}$, a final current density at the time step $l+1/2$ is given by $\mathbf{J} = \mathbf{J}^{(1)} + \mathbf{J}^{(2)}$ for updating the next step electric field. Instead of solving a large matrix with an implicit difference method, the equation of hydrodynamic model is split into a linear explicit equation and a nonlinear explicit equation. The proposed two-step splitting scheme is adopted for efficiency and simplicity of the implementation.

D. Numerical Stability

The stability of the proposed scheme can be analyzed by finding the roots of the corresponding growth matrix. Unfortunately, even with modern computer techniques, expressions for the roots are too complex to obtain. Here, the nonlinear terms in the hyperbolic equation (15) mainly contribute to the high-order harmonic generation. Compared with the linear term in (13), the nonlinear responses are small. After modeling different complex metallic nanostructures for a long-term simulation, we found that the hydrodynamic model was stable within the commonly used CFL constraint of the FDTD method. In other words, the nonlinear terms, which are much weaker than the linear one, do not significantly affect the stability condition of the FDTD method with the linear Drude model.

E. Parallel Strategy

The plasmonic nanodevices, such as metamaterials, are sub-wavelength nanostructures exhibiting a strong near-field enhancement. Simulations of them need a great amount of grids to achieve a high spatial resolution. Meanwhile, the bandwidth of the fundamental pulse should be narrow enough in the frequency domain so that the high-order harmonic signals are not overwhelmed by the fundamental one. As a result, long CPU time with large iteration steps is required to guarantee the sufficient decay of the fundamental pulse. To fix this problem, a parallel computing technique can be employed. Thanks to the localization nature of the FDTD method, we can divide the whole computational domain into many subdomains. A high efficient parallel code can then be achieved by implementing the FDTD code on computer cluster.

Fig. 2 shows our parallel FDTD algorithm. The simulation domain is divided into many subdomains and each subdomain is assigned to a processor. Each subdomain executes the same code in parallel and swaps the data at the interface at every time step. The data exchange between different processors or domains is carried out by using the message passing interface (MPI) library. At the subdomain boundaries, one additional layer of cells is allocated as a swap buffer. The flowchart of the subdomain is diagrammed in Fig. 3. Comparing with the Drude model, the field iterations of the hydrodynamic model need the fields in the neighboring Yee grids, thus the components \mathbf{E} , \mathbf{H} , and \mathbf{J}

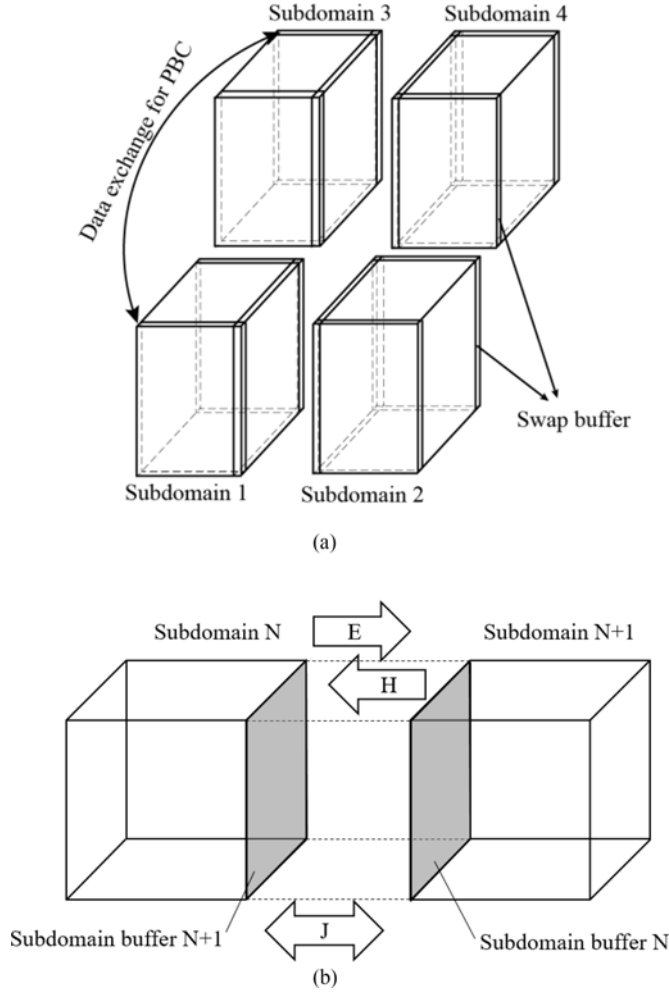


Fig. 2. Diagram of the parallel computing scheme. (a) Parallel FDTD processing on a computer cluster. (b) Field exchange between the adjacent subdomains.

are stored in their swap buffers and exchanged at the interface. In addition, the data exchange is also needed for the periodic boundary condition.

III. NUMERICAL VALIDATION AND APPLICATION

The nonlinearity of plasmonic nanodevices is simulated in this section. This problem is motivated by a recent experiment research [22]. A broadband and efficient THz emission from a plasmonic metasurface is based on resonant photoexcitation of the magnetic dipole resonance. The THz emission from the metamaterials is continuous in the THz regime and its intensity is of the same order as optimal crystals that are thousand times thicker.

A. Configurations

In a recent work, researchers have shown that a THz source ranging from 0.1 to 4 THz can be generated by a plasmonic metasurface [22]. However, due to the upper cutoff frequency of the inorganic crystal detector is much smaller than the emitted THz signal, the measured bandwidth of THz signal was much

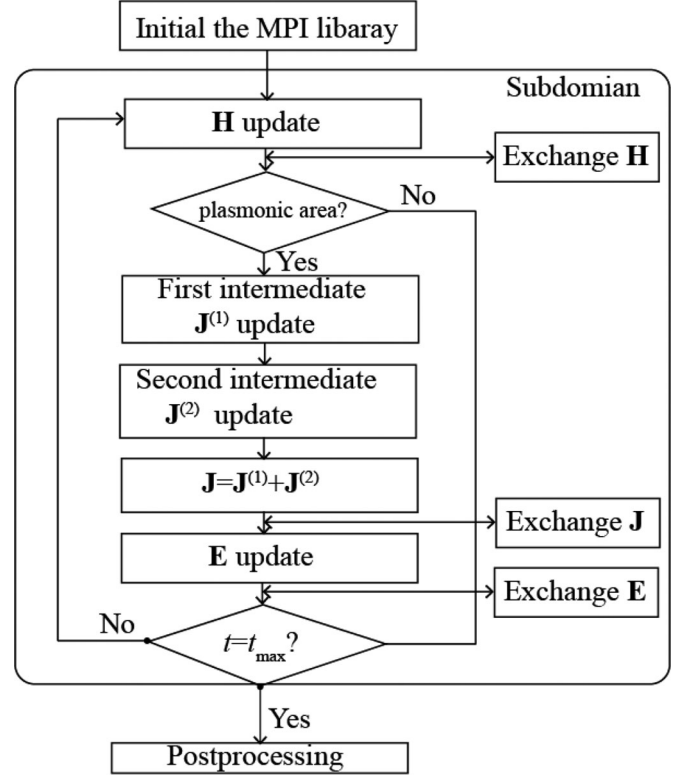


Fig. 3. Flowchart of a subdomain in the parallel FDTD scheme.

narrower than the expected. Therefore, it is important to investigate the mechanism of the THz emission from metasurface by a numerical method. The efficient and compact metasurface THz emitter is shown in Fig. 4(a). The gold SRRs are arranged periodically in both x and y directions and supported by a layer of glass substrate coated with ITO. The thickness of the gold film, ITO, and SiO_2 substrates are 40, 6, and 200 nm, respectively. The glass substrate and ITO layer are chosen as nondispersive dielectric materials and the relative permittivity are 2.25 and 3.8, respectively. The parameters for gold are taken to be $n_0 = 5.92 \times 10^{28} \text{ m}^{-3}$ and $\gamma = 10.68 \times 10^{13} \text{ rad/s}$. The dimensions of the SRRs are chosen as shown in Fig. 4(b).

B. Validation With Linear Response

We first consider the validation for the linear response of our method. The set of (1), (2), (10), and (11) are numerically solved by employing the ADE-FDTD method. A plane wave source is introduced by using the total-field and scattered-field (TF/SF) technique and it propagates in the z -direction. PMLs are set to be in the z -direction and periodic boundary conditions are employed at both the x and y directions. Uniform spatial steps $\Delta x = \Delta y = \Delta z = 2 \text{ nm}$ and a time step $\Delta t = 3 \times 10^{-18} \text{ s}$ are applied. A computational domain of $190 \times 190 \times 1000$ grids is used. The calculated transmittance spectrum of the plasmonic metasurface around the fundamental magnetic resonance frequency is calculated numerically by using the hydrodynamic model and compared with the Drude model as shown in Fig. 5(a). The solid line indicates the spectra obtained by the hydrody-

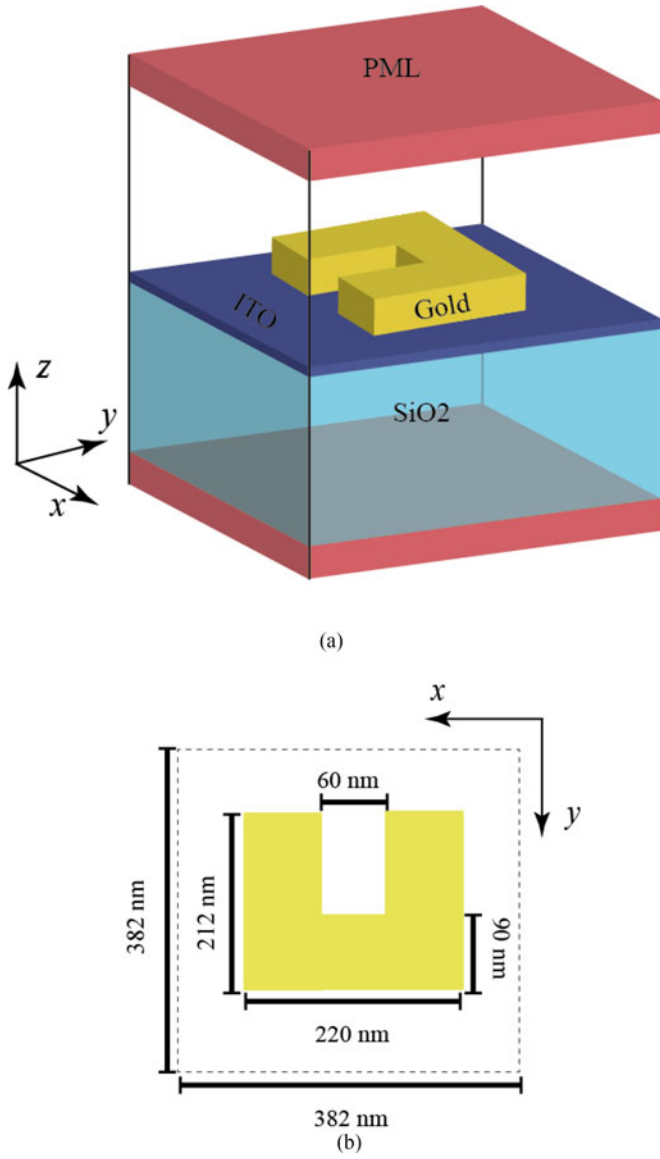


Fig. 4. (a) Layout of a metasurface consist of a periodic array of SRRs. (b) Feature size of a unit cell.

dynamic model and the dashed line is the spectra calculated by the Drude model. Fig. 5(b) shows the relative errors. One can see that the results obtained using our proposed method are in good agreement with those obtained with the classical Drude method.

C. Nonlinear Simulation

The THz emission from the metasurface due to optical rectification or difference-frequency generation is induced by the symmetry breaking in the second-order nonlinear current distribution. From (9), we can see that the convective acceleration terms $(\mathbf{J} \cdot \nabla)\mathbf{J}$ and $(\nabla \cdot \mathbf{E})\mathbf{E}$ are the key contributions to the second-order nonlinearities. These terms behave like linear current times linear charge density $\mathbf{J}\rho$, consequently, the THz nonlinear current is parallel or antiparallel to the linear current. When the polarization of incident wave is parallel to

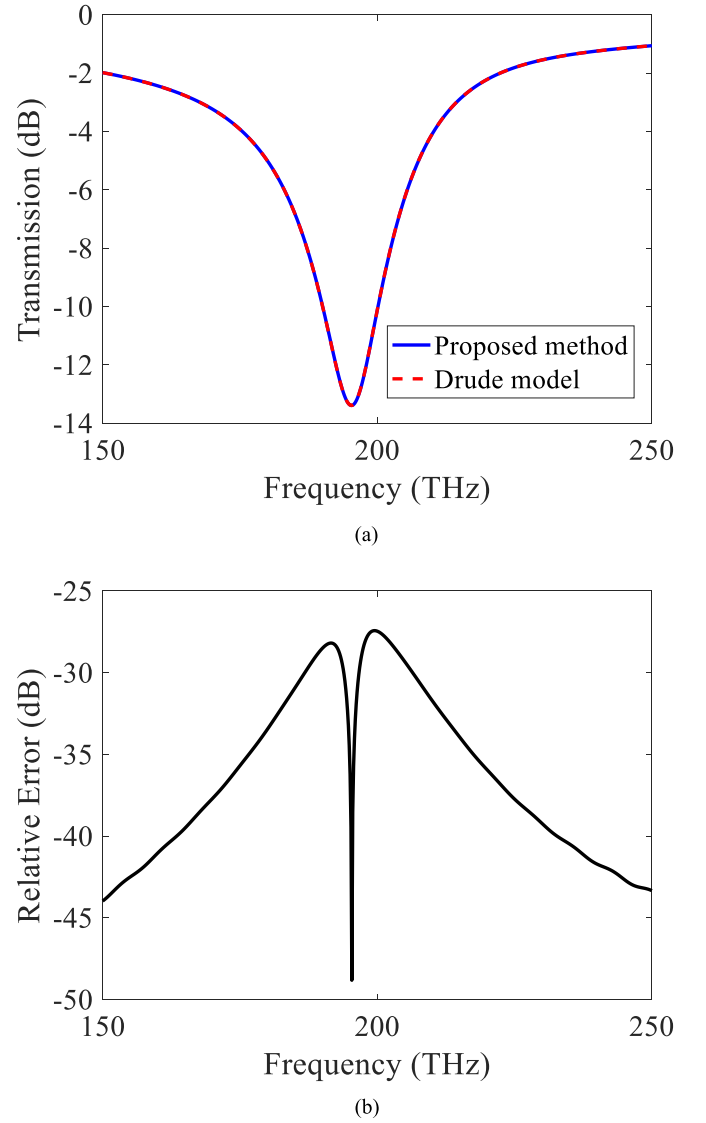


Fig. 5. (a) Calculated transmittance of the metasurface shown in Fig. 4. The results are shown for x -polarized excitation. (b) Relative errors between our method and the Drude model.

the gap of SRRs (x -polarization), the nonlinear currents at both arms are parallel and radiate fields that can be observed in the far field.

To validate the nonlinear response of our method, we model the THz emission from the metasurface that is excited by an x -polarized laser. The pump laser is a Gaussian pulse

$$E(t) = \cos(\omega_0 t + \varphi)g(t) \quad (17)$$

where

$$g_\sigma(t) = e^{-\frac{1}{2}\sigma^2 t^2} \Leftrightarrow g_\sigma(\omega) = \frac{\sqrt{2\pi}}{\sigma} e^{-\frac{\omega^2}{2\sigma^2}} \quad (18)$$

is a Gaussian envelope. ω_0 is the center frequency of the pump pulse and ϕ is a phase delay. The second-order nonlinear polarization from the plasmonic material is proportional to the power

of the incident pump pulse

$$\begin{aligned} P^{(2)}(t) &\sim E^{(2)}(t) \\ &= \cos(2\omega_0 t + 2\phi)g_\sigma^2(t) + g_\sigma^2(t) \end{aligned} \quad (19)$$

$$\begin{aligned} P^{(2)}(\omega) &\sim e^{i2\phi} g_{\sqrt{2}\sigma}(\omega - 2\omega_0) \\ &+ e^{-i2\phi} g_{\sqrt{2}\sigma}(\omega + 2\omega_0) + g_{\sqrt{2}\sigma}(\omega). \end{aligned} \quad (20)$$

Here, the first two terms are corresponding to the second nonlinearity with the center frequency $2\omega_0$; the last term is the THz emission; thus, the THz emission only depends on the temporal Gaussian envelope. The emitted THz field has an analytical solution given by

$$\begin{aligned} E^{THz}(t) &\sim \partial^2 P / \partial t^2 \sim \chi^{(2)} \partial_t^2 g_{\sqrt{2}\sigma}(t) \\ &= \chi^{(2)} \sigma^2 (1 - 2\sigma^2 t^2) e^{-\sigma^2 t^2}. \end{aligned} \quad (21)$$

The linear and nonlinear signals are calculated numerically with the proposed method. The driving frequency, temporal width, change rate, and peak amplitude of the pump laser are chosen as $\omega_0 = 1.228 \times 10^{15}$ rad/s, $\sigma = 2 \ln 2 / \tau$, and $E_0 = 2 \times 10^7$ V/m, respectively. Here $\tau = 150$ fs is the duration of excitation pulse corresponding to a spectral width of 3 THz. The total number of simulation time steps is 4.0×10^5 corresponding to a physical time of 1.2 ps. Fig. 6(a) and (b) shows the temporal profile of linear and nonlinear transmitted field, respectively. The linear and nonlinear spectra are plotted in Fig. 6(c) after the Fourier transform. We can see that the second-harmonic and difference-frequency generation are observed clearly.

The THz signals in the frequency domain are extracted. First, a Fourier transform is performed on the time-domain nonlinear signals, in which a specific frequency range of 0–10 THz is selected, while the intensity of all other frequencies outside the selected window is set to zero. Then, we transform these windowed frequency-domain signals back into its time-domain counterparts. Since the resonance of SRRs is much wider (35.2 THz shown in Fig. 5(a)) compared to the pump pulse width, and thus the emitted THz bandwidth from SRRs is limited by the bandwidth of the incident pump pulse. As a comparison, the predicted result of analytical solution is plotted in Fig. 7, from which excellent agreement can be observed. Note that the THz emission bandwidth of our results is broader than the observed THz spectrum in the experiment [22]. This is because the upper cutoff frequency of the THz signal detector in the experiment is smaller than the theoretical prediction. The metasurface THz emitter can generate broadband THz signals by shortening the pump pulse duration because the single-layer emitter of 40-nm thickness is continuous and free from the quasi-phase-matching limitation at the THz region.

By using the parallel strategy in previous section, the performance of our parallel FDTD code can be improved. For the same configuration of $190 \times 190 \times 400$ grid, the computation speedup versus the number of processors is plotted in Fig. 8. The computations are performed on a workstation with 4 Intel(R) Xeon(R) E5-2680 v2 @ 2.80 GHz CPU (a total of 40

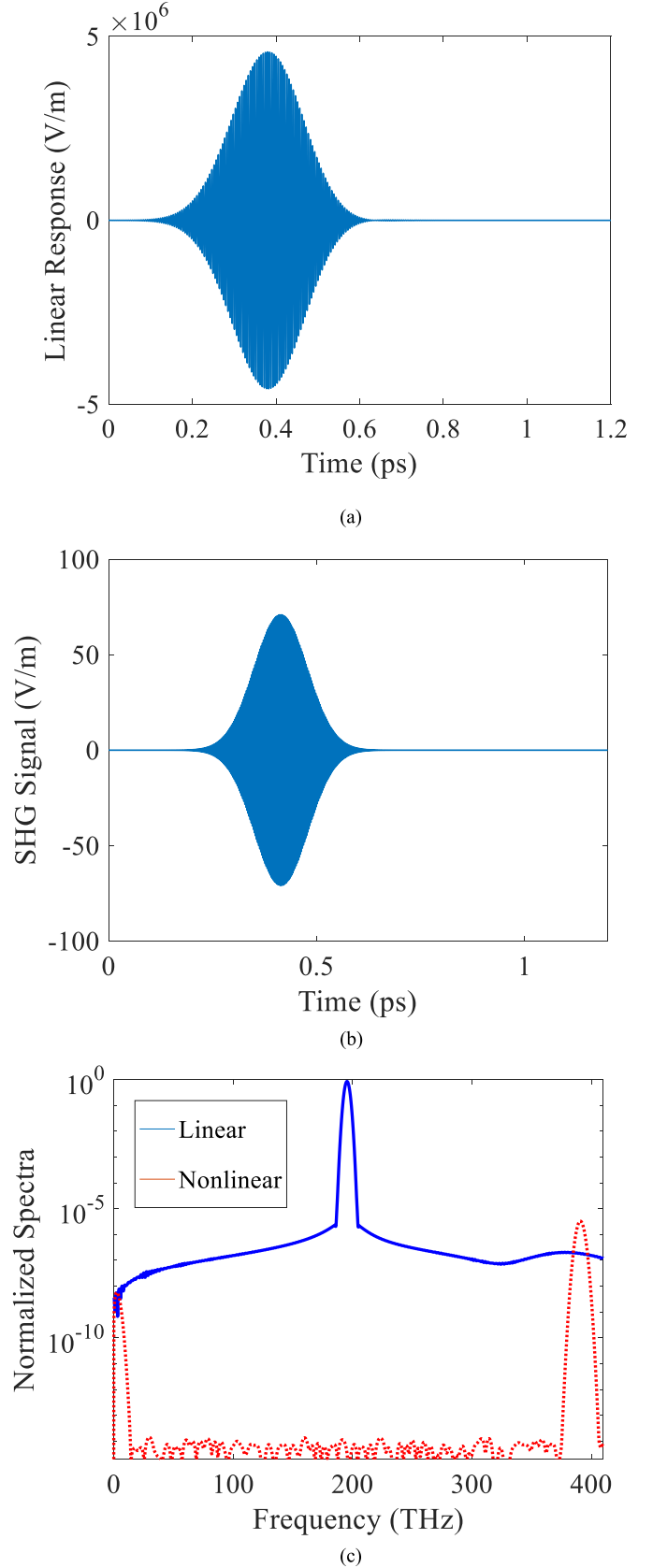


Fig. 6. Electric field as a function of time for (a) linear and (b) nonlinear transmission. (c) Semi-log plot of the Fourier transform of the linear and nonlinear transmitted fields versus frequency.

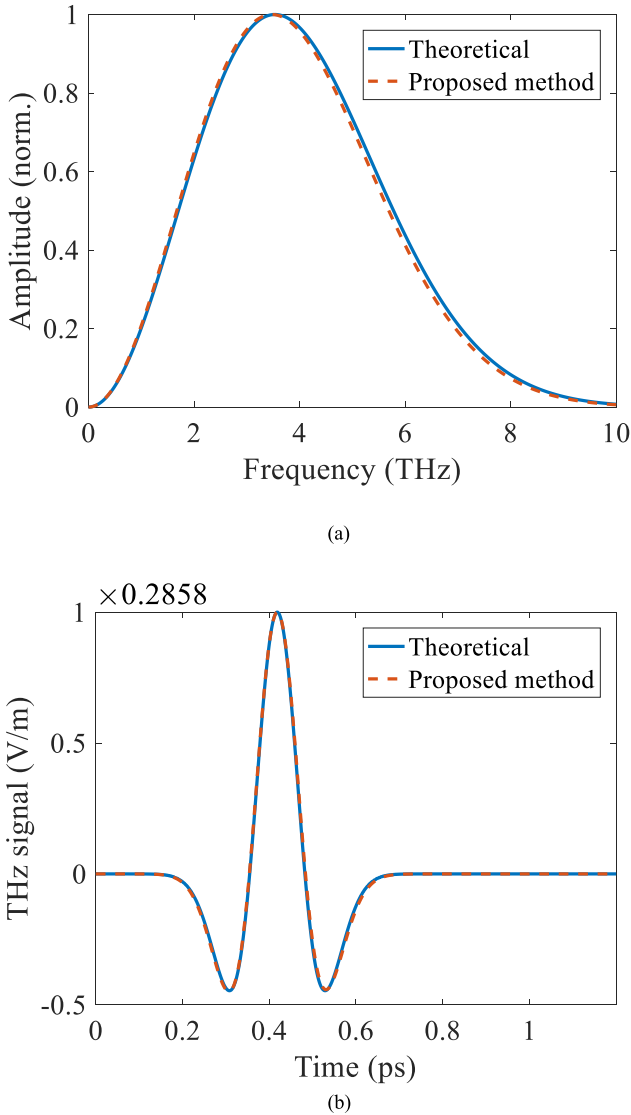


Fig. 7. (a) Normalized THz spectrum and (b) corresponding time-domain THz pulse.

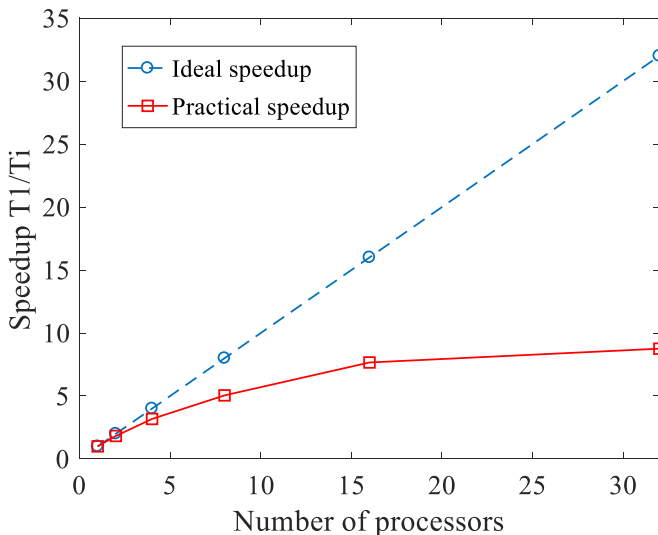


Fig. 8. Computational speedup versus number of processors.

CPU cores). The total computational memory was about 5.4 GB and total computational time was about 20 h with 32 processors. The practical speedup is lower than theoretically expected. This is due to the increased data transfers (**E**, **H**, **J**) between processors. In addition, the implementation in the plasmonic material area is complicated, the simulation time is much large for the subdomain with plasmonic structures. Therefore, simulations of the subdomains decrease the parallel computational efficiency.

IV. CONCLUSION

In conclusion, a self-consistent, accurate, and explicit FDTD-based Maxwell–hydrodynamic model has been developed for investigating and modeling both linear and nonlinear electromagnetic responses in plasmonic metasurfaces. In particular, a time-splitting scheme is adopted for solving the hydrodynamic equation. With the proposed method, the linear transmittance of a plasmonic metasurface is simulated and compared with the Drude model, and the emitted nonlinear THz signal is accurately solved. Consequently, the proposed multiphysics FDTD scheme presents a way for understanding and designing nonlinear plasmonic nanodevices.

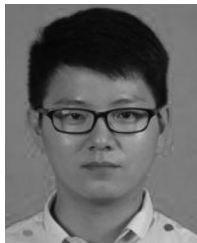
ACKNOWLEDGMENT

Author M. Fang would like to thank C. M. Soukoulis and Th. Koschny for their help and guidance at Iowa State University, Ames, IA, USA.

REFERENCES

- [1] C. M. Soukoulis and M. Wegener, "Past achievements and future challenges in the development of three-dimensional photonic metamaterials," *Nature Photon.*, vol. 5, no. 9, pp. 523–530, Sep. 2011.
- [2] L. Novotny and N. van Hulst, "Antennas for light," *Nature Photon.*, vol. 5, no. 2, pp. 83–90, Feb. 2011.
- [3] S. Linic, P. Christopher, and D. B. Ingram, "Plasmonic-metal nanostructures for efficient conversion of solar to chemical energy," *Nature Mater.*, vol. 10, no. 12, pp. 911–921, Dec. 2011.
- [4] S. P. Burgos, H. W. Lee, E. Feigenbaum, R. M. Briggs, and H. A. Atwater, "Synthesis and characterization of plasmonic resonant guided wave networks," *Nano Lett.*, vol. 14, no. 6, pp. 3284–3292, Jun. 2014.
- [5] M. Fang, Z. Huang, Th. Koschny, and C. M. Soukoulis, "Electrodynamic modeling of quantum dot luminescence in plasmonic metamaterials," *ACS Photon.*, vol. 3, no. 4, pp. 558–563, Apr. 2016.
- [6] A. V. Zayats, I. I. Smolyaninov, and A. A. Maradudin, "Nano-optics of surface plasmon polaritons," *Phys. Rep. Rev. Sect. Phys. Lett.*, vol. 408, no. 3–4, pp. 131–314, Mar. 2005.
- [7] U. Kreibitz, G. Bour, A. Hilger, and M. Gartz, "Optical properties of cluster-matter: Influences of interfaces," *Phys. Status Solidi A Appl. Mater. Sci.*, vol. 175, no. 1, pp. 351–366, Sep. 16, 1999.
- [8] G. Bachelier, I. Russier-Antoine, E. Benichou, C. Jonin, and P. F. Brevet, "Multipolar second-harmonic generation in noble metal nanoparticles," *J. Opt. Soc. Amer. B, Opt. Phys.*, vol. 25, no. 6, pp. 955–960, Jun. 2008.
- [9] J. Butet, I. Russier-Antoine, C. Jonin, N. Lascoux, E. Benichou, and P. F. Brevet, "Sensing with multipolar second harmonic generation from spherical metallic nanoparticles," *Nano Lett.*, vol. 12, no. 3, pp. 1697–1701, Mar. 2012.
- [10] S. Kim, J. H. Jin, Y. J. Kim, I. Y. Park, Y. Kim, and S. W. Kim, "High-harmonic generation by resonant plasmon field enhancement," *Nature*, vol. 453, no. 7196, pp. 757–760, Jun. 5, 2008.
- [11] Y. S. Kivshar, T. J. Alexander, and S. K. Turitsyn, "Nonlinear modes of a macroscopic quantum oscillator," *Phys. Lett. A*, vol. 278, no. 4, pp. 225–230, Jan. 1, 2001.
- [12] X. Y. Z. Xiong, L. J. Jiang, W. E. I. Sha, Y. H. Lo, and W. C. Chew, "Compact nonlinear yagi-uda nanoantennas," *Sci. Rep.*, vol. 6, Jan. 7, 2016, Art. no. 18872.

- [13] X. Y. Z. Xiong *et al.*, "Strongly enhanced and directionally tunable second-harmonic radiation from a plasmonic particle-in-cavity nanoantenna," *Phys. Rev. A, Gen. Phys.*, vol. 94, no. 5, Nov. 14, 2016, Art. no. 053825.
- [14] P. Ginzburg, A. V. Krasavin, G. A. Wurtz, and A. V. Zayats, "Nonperturbative hydrodynamic model for multiple harmonics generation in metallic nanostructures," *ACS Photon.*, vol. 2, no. 1, pp. 8–13, Jan. 2015.
- [15] M. Fang, K. K. Niu, Z. X. Huang, W. E. I. Sha, and X. L. Wu, "Modeling nonlinear responses in metallic metamaterials by the FDTD solution to Maxwell-hydrodynamic equations," in *Proc. 2016 IEEE Int. Conf. Comput. Electromagn.*, 2016, pp. 4–6.
- [16] C. Ciraci, E. Poutrina, M. Scalora, and D. R. Smith, "Origin of second-harmonic generation enhancement in optical split-ring resonators," *Phys. Rev. B, Condens. Matter*, vol. 85, May 15, 2012, Art. no. 201403(R).
- [17] J. Butet, B. Gallinet, K. Thyagarajan, and O. J. F. Martin, "Second-harmonic generation from periodic arrays of arbitrary shape plasmonic nanostructures: A surface integral approach," (in English), *J. Opt. Soc. Amer. B, Opt. Phys.*, vol. 30, no. 11, pp. 2970–2979, Nov. 2013.
- [18] K. S. Yee, "Numerical solution of initial boundary value problems involving Maxwell's equations in isotropic media," *IEEE Trans. Antennas Propag.*, vol. AP-14, no. 3, pp. 302–307, May 1966.
- [19] M. Fujii, M. Tahara, I. Sakagami, W. Freude, and P. Russer, "High-order FDTD and auxiliary differential equation formulation of optical pulse propagation in 2-D Kerr and Raman nonlinear dispersive media," *IEEE J. Quantum Electron.*, vol. 40, no. 2, pp. 175–182, Feb. 2004.
- [20] A. S. Nagra and R. A. York, "FDTD analysis of wave propagation in nonlinear absorbing and gain media," *IEEE Trans. Antennas Propag.*, vol. 46, no. 3, pp. 334–340, Mar. 1998.
- [21] M. Fujii, M. Tahara, I. Sakagami, W. Freude, and P. Russer, "High-order FDTD and auxiliary differential equation formulation of optical pulse propagation in 2-D Kerr and Raman nonlinear dispersive media," *IEEE J. Quantum Electron.*, vol. 40, no. 2, pp. 175–182, Feb. 2004.
- [22] L. Luo *et al.*, "Broadband terahertz generation from metamaterials," (in English), *Nature Commun.*, vol. 5, Jan. 2014, Art. no. 3055.
- [23] J. Liu *et al.*, "Generalization of the FDTD algorithm for simulations of hydrodynamic nonlinear Drude model," *J. Comput. Phys.*, vol. 229, pp. 5921–5932, 2010.
- [24] M. Fang, Z. Huang, W. E. I. Sha, X. Y. Z. Xiong, and X. Wu, "Full hydrodynamic model of nonlinear electromagnetic response in metallic metamaterials," *Progress Electromagn. Res.*, vol. 157, pp. 63–78, 2016.



Ming Fang was born in Anhui, China, in 1990. He received the B.S. and M.S. degrees from the School of Electronics and Information Engineering, Anhui, China, in 2011 and 2014, respectively, and is currently working toward the Ph.D. degree at Iowa State University, Ames, IA, USA.

From March 2015 to August 2015, he was a Research Assistant with the Department of Electrical and Electronic Engineering, University of Hong Kong, Hong Kong. His research interests include multiphysics modeling with time-domain numerical

methods, metamaterials, and nonlinear optics. Dr. Fang was the recipient of the Honorable Mention of the 2015 IEEE MTT-S International Conference on Numerical Electromagnetic and Multiphysics Modeling and Optimization Student Paper Competition, Ottawa, ON, Canada, in 2015.



Zhixiang Huang (M'16) was born in Anhui, China, in 1979. He received the B.S. and Ph.D. degree from Anhui University, Hefei, China, in 2002 and 2007, respectively.

From 2010 to 2011, he was a Visiting Scholar with Iowa State University, Ames, IA, USA. His research interests include time-domain numerical methods, metamaterial, and active metamaterials.

He is a member of the OSA.



Wei E. I. Sha (M'09–SM'17) received the B.S. and Ph.D. degrees in electronic engineering from Anhui University, Hefei, China, in 2003 and 2008, respectively.

From July 2008 to May 2012, he was a Post-doctoral Research Fellow with the Department of Electrical and Electronic Engineering, University of Hong Kong, Hong Kong, where he is currently a Research Assistant Professor. He is the coauthor of two books on the finite-difference time-domain method and wavelet theory. He has authored or co-authored

90 peer-reviewed journal papers included in the Web of Science Core Collection. He also contributed 4 book chapters for Springer, CRC Press, and InTech Publishers and 16 invited talks at international conferences. He engages in theoretical and computational research in electromagnetics and optics focusing on multiphysics and interdisciplinary research. The research topics are inspired by applications in several areas including solar energy, microwave/optical communication, sensing/detection, and quantum information. His research interests include fundamental and applied aspects in plasmonics, emerging photovoltaics, metasurfaces, quantum electrodynamics, and computational electromagnetics.

Dr. Sha is an OSA member. In 2007, He was the recipient of the Marie Skłodowska-Curie Individual Fellowship of European Commission and the Thousand Talents Program for Distinguished Young Scholars of China in 2007. He was the recipient of the Chinese Youth Science and Technology Innovation Prize in 2007. He and his collaborators were the recipients of the Research Output Prize of the University of Hong Kong in 2013, the Outstanding Reviewer of the *Journal of Computational Physics* in 2014, the Second Prize of Science and Technology from the Anhui Province Government, China, and four Best Student Paper Prizes and one Young Scientist Award with his students. He served on the Onsite Award Committee and Technical Program Committee or as Session Chair of several international conferences including ACES 2017, ICCEM 2017/2016, PIERS 2016, IMWS-AMP 2015, etc. He is currently an Invited Referee of IEEE, OSA, AIP, APS, and Nature Publishing Group journals. He was a Book Proposal Reviewer for CRC Press and Bentham Science publishers and an Official Reviewer for the PRESTIGE Marie Curie Postdoc Fellowships Programme.



Xianliang Wu (M'09) was born in Bozhou, China, in 1955. He received the B.S. degree in electronic engineering from Anhui University, Hefei, China, in 1982.

He is currently a Full Professor with the Department of Electronic Engineering, the Director of the Laboratory of Electromagnetic Field and Microwave Technology, Anhui University, and the Principal of Hefei Normal University, Hefei, China. He has authored or co-authored more than 100 papers and 3 books. His research interests include electromagnetic

field theory, electromagnetic scattering and inverse scattering, and wireless communication.

Prof. Wu is a Senior Member of the Chinese Institute of Electronics. He is an Associate Director of the Chinese Institute of Microwave Measurement.